

## ON-ORBIT INVESTIGATION OF TRANSIENT MICRODYNAMIC DISTURBANCES ON A DEPLOYED TRUSS STRUCTURE

Michel D. Ingham\*  
 Space Systems Laboratory  
 Massachusetts Institute of Technology  
 77 Massachusetts Ave., Rm. 37-356  
 Cambridge, MA 02139  
 ingham@mit.edu

Marie B. Levine†  
 Jet Propulsion Laboratory  
 California Institute of Technology  
 4800 Oak Grove Dr., M.S. 157-316  
 Pasadena, CA 91109  
 marie.levine@jpl.nasa.gov

### ABSTRACT

The second Interferometry Program Experiment (IPEX-2) is a technology demonstration precursor to the Space Interferometry Mission, a 10-meter baseline space-based interferometer scheduled for launch in 2005. The main objective of the IPEX-2 flight experiment is to ascertain the existence of transient disturbances originating within mechanisms, joints and materials, due to sudden internal strain energy redistribution. Results from this on-orbit microdynamic investigation of a representative deployed truss structure are presented, along with a summary of the finite element modeling work performed on the IPEX-2 structure. The experimental results demonstrate the existence of broadband transient disturbances believed to have resulted from thermally-induced vibrations in the structure (*thermal creaks*). A quantitative characterization of these disturbances is performed, revealing peak acceleration response levels between 300  $\mu\text{g}$  and 700  $\mu\text{g}$ , in general. The corresponding peak integrated displacements are generally less than 50 nm in amplitude. Microdynamic response to known disturbance sources such as flight data recorders, gyros and thrusters are also characterized.

### 1 INTRODUCTION

The second Interferometry Program Experiment (IPEX-2) is a space flight experiment investigating the microdynamic behavior of a representative deployed truss structure. This experiment serves as a technology dem-

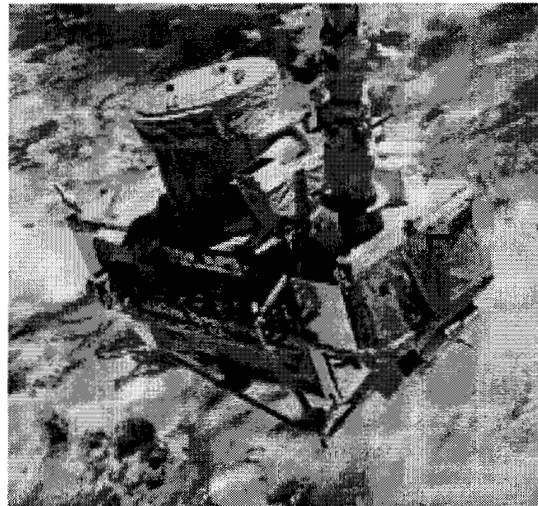


FIG. 1: Astro-SPAS and IPEX-2 on-orbit.

onstration for the planned space telescopes in NASA's Origins Program, including the Space Interferometry Mission (SIM). IPEX-2 was flown on the STS-85 Shuttle Mission in August 1997, as a secondary payload mounted on the free-flying DaimlerChrysler Aerospace/DARA satellite pallet, Astro-SPAS. Figure 1 shows a photograph of the Astro-SPAS with the IPEX-2 test article, on-orbit. The main objective of this experiment is to demonstrate and characterize the occurrence of impulsive microdynamic-level disturbances, as a result of changes in the internal stress distribution of a statically indeterminate structure with nonlinear frictional mecha-

\* Graduate Research Assistant, Student Member AIAA

† Microdynamics Project Element Manager, Space Interferometry Mission, Member AIAA

nisms. Secondary objectives of the IPEX-2 experiment are determination of the dynamic properties of the flight test article on-orbit, and determination of the dynamic response and propagation attenuation of known mechanical disturbances. Some preliminary results from the flight experiment have been previously published<sup>1,2</sup>. This paper updates those results and presents a summary of the IPEX-2 modeling and data analysis work completed to date.

In this experiment, the type of microdynamic disturbance most likely to occur is thermal creak, which is a result of quasi-static or dynamic slip across a discontinuous interface. Non-uniform thermal loading across a structure, or mismatch in the coefficients of thermal expansion (CTE) between different components changes the normal-to-shear load distribution across discontinuous interfaces such as hinges, latches and joints. This leads to changes in the stress distribution which result in microslip or gross dynamic motion. It should be noted that interface slips are not only thermally-induced phenomena. Temperature variations are just one of the ways that loads can be applied to a structure. Slips can also occur from mechanical load redistribution within a system, such as would happen during configuration changes (e.g., deployment, moving components).

Recent work in the fields of microdynamic characterization and modeling of structures with nonlinear mechanisms is shedding light on the sources of thermal creak in space structures. Investigations of microslip mechanisms and the phenomenon of thermal creak have been performed at the University of Colorado<sup>3,4,5</sup> and at MIT<sup>6,7</sup>. Thermal creak is a disturbance of particular concern to engineers designing spacecraft with tight dimensional stability requirements, such as SIM. For instance, on-orbit data from the Hubble Space Telescope revealed transient disturbances, which were attributed to thermally-induced creaking<sup>8</sup>. Ongoing work at the University of Colorado and NASA Langley Research Center is focusing on the design of microdynamically stable mechanisms, which would render structures less susceptible to creaking behavior<sup>9,10</sup>.

## **2 EXPERIMENT DESCRIPTION**

This section provides a brief description of the IPEX-2 flight experiment, including the structural test article, instrumentation and flight experiment profile. A description of the IPEX-2 hardware and experiment configuration can also be found in previously-published papers<sup>1,2</sup>.

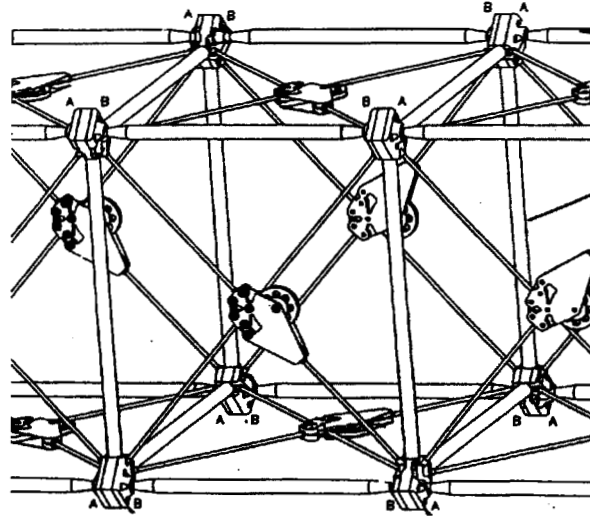


**FIG. 2:** Close-up view of single bay.

The second Interferometry Program Experiment, IPEX-2, flew on shuttle mission STS-85, in August 1997. IPEX-2 was a secondary payload on the reusable science satellite Astro-SPAS (A/S). The Astro-SPAS is a spacecraft developed by DaimlerChrysler Aerospace, which is launched into Earth orbit by the Space Shuttle and deployed for a free flight period of approximately 10 days. During IPEX-2, a nine-bay joint-dominated pre-loaded truss was cantilevered off the side of the CRISTA-SPAS (Figure 1). The truss is made up of graphite composite longerons and battens, with stainless steel cables and fittings. A close-up view of one bay is shown in Figure 2. Roughly 300 lbf of pretension in the diagonal cables result in compressive preloads of approximately 400 lbf and 430 lbf in the longerons and battens, respectively. The end-to-end length of the boom is approximately 92 inches. The geometric and material properties of the boom have been fully documented<sup>11</sup>.

The truss design incorporates numerous joints and mechanisms, which represent possible creak sources. Furthermore, there is a significant mismatch in the coefficients of thermal expansion of the composite truss members and the steel diagonal cables. This mismatch, coupled with the statically indeterminate design of the boom and the changing thermal environment on-orbit, provide the strain energy storage mechanism required for thermal creak behavior.

The instrumentation used to perform the on-orbit dynamic and thermal characterization of the structure includes 24 micro-g accelerometers, 8 load cells, 48 temperature sensors, and 2 proof-mass actuators. Six of

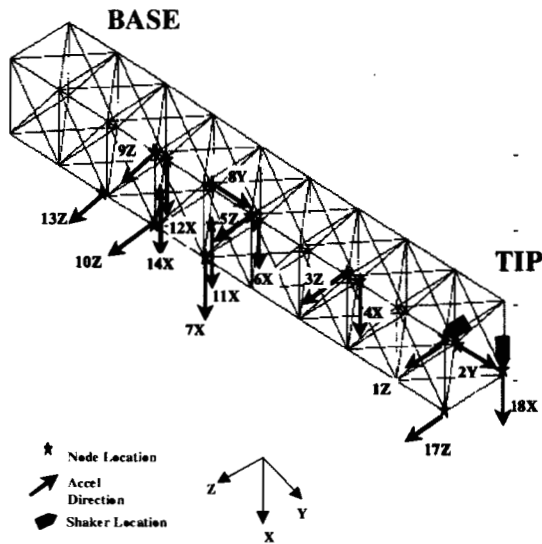


FIG. 3: Boom-mounted accelerometer locations.

the accelerometers and six load cells were collocated inside the boom-to-spacecraft interface (I/F) struts to characterize the six interface degrees-of-freedom. Sixteen accelerometers were installed along the boom (Figure 3), including two that were collocated with the two shakers and load cells at the tip of the boom. The shakers were used to perform on-orbit modal tests to characterize the linearity and modal properties of the boom. The remaining two accelerometers were installed on the A/S so as to provide information on the source of any vibrations measured on the boom. Of the 48 temperature sensors, 24 were located inside the accelerometer casings for calibration purposes, and the remaining 24 were distributed along the boom as follows: 16 collocated on the corner fittings with the accelerometers to monitor the ambient temperature in the event of a thermal creak, 2 placed on either side of a longeron truss member to investigate thermal gradients across the member, 2 placed on either side of a batten truss member, 3 placed on the pulley plate fittings, and 1 placed on a corner fitting near the base of the boom.

Close to 50 hours of on-orbit data was recorded at a 1 kHz sampling rate with 16-bit accuracy, representing approximately 10 gigabytes of storage space. The overall noise floor is estimated to be 20  $\mu\text{g}$  RMS up to 500Hz, with 1  $\mu\text{g}$  RMS below 10 Hz. During the first 45 hours, the response of the boom during normal A/S operation modes was recorded. The active disturbance sources include gyros, thrusters, and other payloads. This period also included over 25 day/night and night/

day transitions. A preliminary assessment of this period has been previously reported<sup>1</sup>.

The last 5 hours of the A/S flight were specifically dedicated to IPEX-2; all other payloads were turned off. During this IPEX-dedicated period, a total of 14 multi-shaker modal tests were performed to assess the on-orbit structural dynamic properties of the boom. Two experiments were also dedicated to evaluating the boom response to specific A/S mechanical disturbances: gyro response without thrusters (the "quiescent gyro experiment"), and thruster pulsing with and without the gyros in the background (the "thruster pulsing experiment"). Data from these experiments are discussed briefly in Section 4 of this paper.

The most important IPEX-2 experiment corresponds to one 5-minute segment, during which even the A/S gyros and thrusters were shut down, and the boom experienced a sudden night to day transition. The only active mechanism on board was the flight data recorder. This "quiescent period" provides the minimum disturbance state of the A/S, and is the period most likely to be quiet enough to measure thermally induced microdynamics in the boom. This period is the focus of most of the flight data analysis performed to date, to be discussed in Section 4 of this paper.

### 3 MODELING

Finite element (FE) models of the IPEX-2 structure in its ground and flight configurations were built, for use in the dynamic analysis and data visualization tasks. Thorough descriptions of the different models created are available in previously released documents<sup>11,12</sup> and thus only a brief summary of the most significant results from the most recent model is presented here.

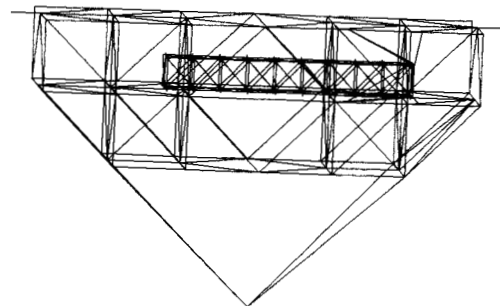


FIG. 4: Coupled SPAS/boom model.

Figure 4 depicts a finite element model of the boom, coupled with a model of the Astro-SPAS platform. Modal frequencies from this coupled model are tabulated in Table 1 (column labeled 'Nominal Model; 25 deg C; 0-g'). The nominal model is assumed to be unconstrained, in 0-g and room temperature conditions.

The effect of on-orbit temperature loads was investigated, by applying a -65 deg C temperature change to the nominal model. The modal frequencies listed in Table 1 show that the first bending modes of the boom are essentially unchanged by the temperature load. The fundamental torsion mode is softened, going from 29.7 Hz down to 28.2 Hz. Not surprisingly, the SPAS-dominated modes are unaffected by the change in boom pre-load induced by the temperature change, while the frequencies of the diagonal drum modes increase. The application of the temperature load results in modes in which torsion, bending and A/S deformations are more highly coupled.

It is important to note that changes in internal stress distribution will affect potential creak mechanisms: the greater the change in internal load from the nominal loading condition, the sooner the critical load for slip of the nonlinear frictional mechanisms will be reached. Such changes in internal stress can arise due to a number of different sources, such as thermal load on a statically indeterminate structure with CTE mismatch, or on-orbit operations-induced mechanical load redistribution.

In order to investigate the effect of model fidelity on the modes, several modeling details were added to the nominal model, to better represent the actual system flown, e.g. the cable tray and the SPAS-mounted Experiment Support Plate (ESP) supporting the free end latch/plunger mechanism. The modal frequencies up to 100 Hz from this detailed coupled model are presented in the last column of Table 1, for 0-g and room temperature conditions. The first three flexible modes are essentially unchanged from the nominal model. However, the addition of the cable tray and ESP plate results in extra modes at 45.9, 47.2 and 58.8 Hz, which were not found in the nominal model. For both the nominal and detailed models, the global boom modes found in the 60 to 98 Hz range are coupled with local "drumming" of the pulley fittings on the diagonal cables, and also sometimes with SPAS deformations. The mode shapes and frequencies in this range are more significantly affected than the fundamental bending and torsion modes, due to the addition of the above-mentioned modeling details.

**TABLE 1: Flexible modes of the coupled model, up to 100 Hz (frequencies in Hz)**

| Description  | Nominal model<br>25 degC<br>0-g | Nominal model<br>-40 degC<br>0-g | Detailed model<br>25 degC<br>0-g |
|--|---------------------------------|----------------------------------|----------------------------------|
| B: boom bending<br>T: boom torsion                             |                                 |                                  |                                  |
| B1   | 12.5                            | 12.5                             | 12.5                             |
| B1   | 18.4                            | 18.4                             | 18.4                             |
| T1   | 29.7                            | 28.2                             | 29.7                             |
| SPAS-dominated modes (some coupled with B & T)                 | 34.8                            | 34.8                             | 35.3                             |
|  | 39.8                            | 39.8                             | 39.6                             |
|  | 41.2                            | 41.2                             | 41.2                             |
|  | 48.5                            | 48.5                             | 45.9                             |
|  |                                 |                                  | 47.2                             |
|  |                                 |                                  | 48.5                             |
| Diagonal drum modes (accels A11 & A14)                         | 54.6                            | 54.8                             | 54.7                             |
|  | 54.9                            | 60.0                             | 55.0                             |
|  | 56.6                            | 60.9                             | 56.6                             |
|  |                                 | 61.6                             |                                  |
|  |                                 | 65.4                             |                                  |
| SPAS & ESP plate mode  | -                               | -                                | 58.8                             |
| Diagonal drum modes (some coupled with B,T, & A/S deformation) | 60.0                            | 66.3                             | 61.3                             |
|  | up to 97.7                      | up to 97.6                       | up to 98.1                       |

#### **4 FLIGHT DATA ANALYSIS**

Approximately 10 gigabytes of data were recorded during the IPEX-2 flight experiment, much of which remains to be analyzed. To date, analysis effort has mainly focused on the five-minute quiescent period. The applicability of various data mining techniques is under investigation, in hopes of automating the difficult and lengthy task of cataloguing the numerous disturbances seen throughout the remaining 50 hours or so of data.

In this section, an overview of the flight data analysis is presented. First, the quiescent period data will be addressed, including summaries of both the dynamic and thermal data analyses performed to date. The next two five-minute data segments immediately following the quiescent period will then be discussed, in order to ascertain the continuity of a number of disturbances seen during the quiescent period, and to characterize some known disturbance sources.

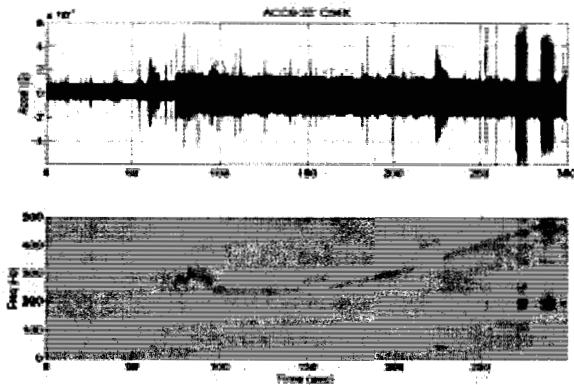


FIG. 5: Time history and spectrogram for the quiescent period, obtained at accelerometer A4.

#### 4.1 Quiescent Period

The quiescent period represents the minimal disturbance state of the boom, in which microdynamic behavior is most likely to be observed above the background or sensor noise. A typical time history of this period, measured on an accelerometer mounted transversely to the boom's longitudinal axis, is shown in Figure 5. A spectrogram of the time history is also included to illustrate

the time-varying nature of the frequency content of the disturbances. As can be seen, the flight data is rich in dynamic response: forty-five different types of events were identified. A detailed catalog of the events picked up by the sensors during this period has been compiled<sup>13</sup>. These events included steady-state disturbances, transient disturbances, and disturbances with time-varying frequency content. Based on analysis of the data thus far, a number of the quiescent period transient disturbances have been identified as possible thermal creaks. In this paper, detailed analysis results are described for a representative selection of events. A complete overview of the analysis results from the quiescent period data can be found in other documents<sup>13,14</sup>.

One of the main goals of the IPEX flight experiment is to provide future precision structures, such as JPL's Space Interferometry Mission (SIM), with an idea of the RMS, peak amplitudes and frequency content of microdynamic disturbances expected on-orbit. Although such disturbances are generally specific to a particular structure, the IPEX results can offer reasonable, representative "first-cut" estimates for microdynamic disturbance levels, which may be used as inputs to an integrated model of the spacecraft and instrument. An appropriate way to translate these measured accelerations into inputs for a model is under investigation.

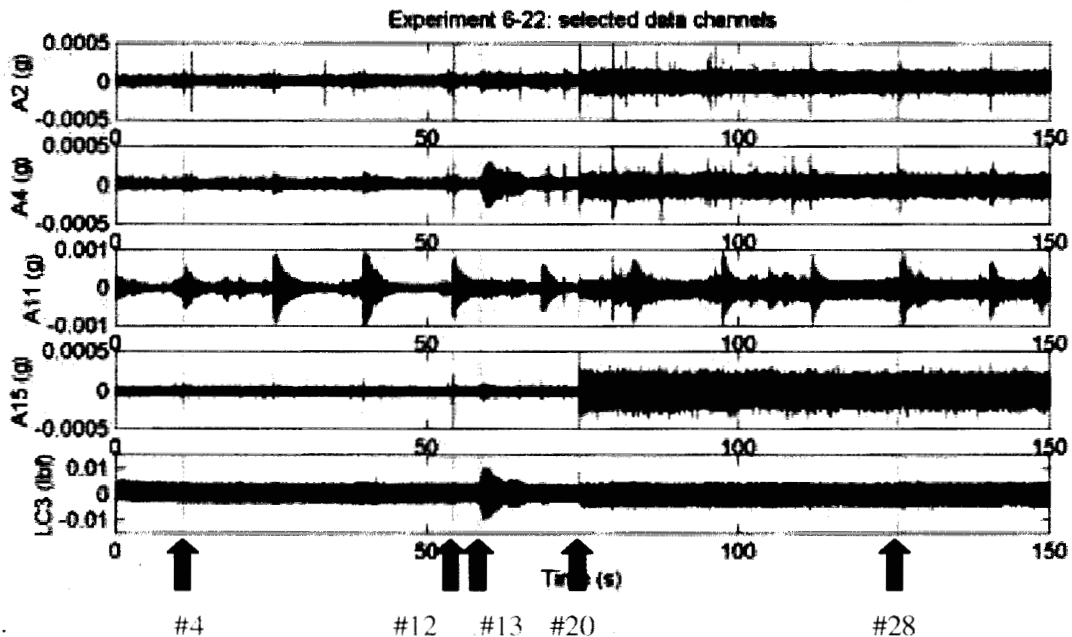


FIG. 6: Quiescent period time histories from various sensors (arrows indicate selected events seen in the data). The numbering labels associated with each arrow correspond to the numbering scheme used in the Event Catalog<sup>13</sup>.

Figure 6 presents time history data from five different sensors, corresponding to the first 150 seconds of the 5-minute quiescent period. The first four time traces are from accelerometers. A2 and A4 were located on the boom as shown in Figure 3, oriented longitudinally and transversely with respect to the boom axis, respectively. A11 was mounted to a pulley fitting at the center of a bay face. A15 was mounted on the A/S, near the base of the boom. The fifth time trace is from one of the load cells internal to the interface struts providing attachment between the boom and the A/S. It is evident from this figure that the nature and amplitude of the response to each event varies quite significantly across the structure. For example, the response measured on the pulley fitting (A11) is dominated by ringing at the frequency of the transverse drum mode for the pretensioned diagonal cables, whereas the other boom-mounted accelerometers see more short-duration, high-frequency transients. In general, fewer events are seen on the load cells and SPAS-mounted accelerometers.

Of the many different events seen during the quiescent period, five have been selected as representative, or particularly interesting. The vertical dotted lines and arrows in Figure 6 indicate these five events. In the following discussion, each of these events will be characterized in further detail, in both the time and frequency domains. It should be noted that the numbering scheme used to label these events corresponds to the numbering scheme used in the IPEX-2 Quiescent Period On-Orbit Event Catalog document<sup>13</sup>.

Requirements for precision structures such as SIM are often expressed in terms of displacement, or velocity, rather than acceleration. The velocities for the five selected events have been computed from the acceleration response data, by high-pass filtering the signals to eliminate the DC component (and low-frequency electronic noise) and numerically integrating. The filtering and integration process was then repeated on the resulting velocity time histories to obtain displacements. Unless otherwise indicated, a high-pass filter with corner frequency at 23 Hz was used. Figures 7 through 11 show acceleration, velocity and displacement time traces for the five representative disturbances indicated on Figure 6.

Throughout the flight data, transient events are seen on most of the sensor channels, every 14.4 seconds. These events are associated with structural response to a periodic disturbance: the rotary mechanism of the flight data recorder. The acceleration, velocity and displacement traces for a typical flight data recorder disturbance (Disturbance #4 from the Event Catalog<sup>13</sup>), as measured at

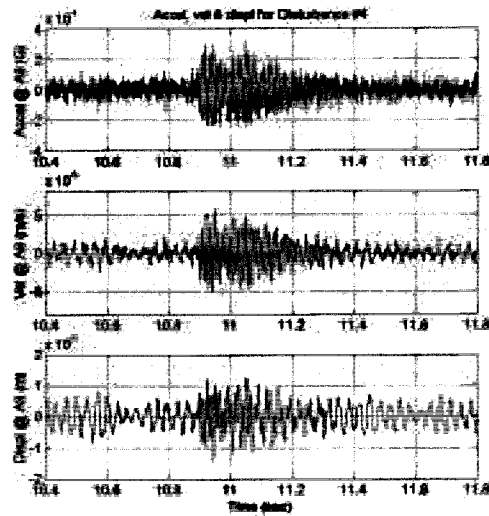


FIG. 7: Acceleration, velocity & displacement for tape recorder Disturbance #4 (boom accelerometer A9).

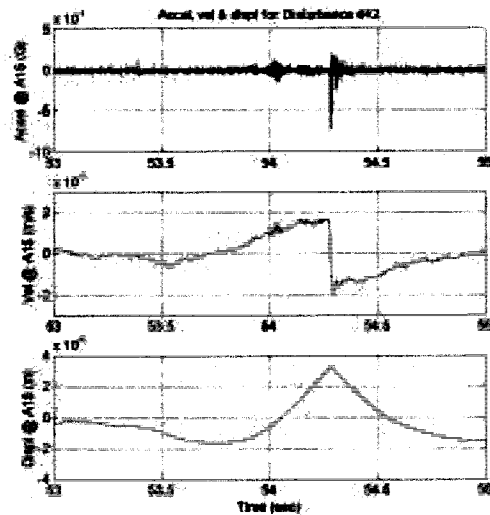


FIG. 8: Acceleration, velocity & displacement for impulsive Disturbance #12, with assumed A/S source (SPAS accelerometer A15).

boom-mounted accelerometer A9, are shown in Figure 7. The disturbance is evident in all three traces. The peak acceleration observed on the structure is around  $314 \mu\text{g}$ , while the velocity reaches  $5 \mu\text{m/s}$ , and the displacement peaks just under  $15 \text{ nm}$ . In general, the frequency content of the response to the tape recorder disturbance is focused in the 60-100 Hz band.

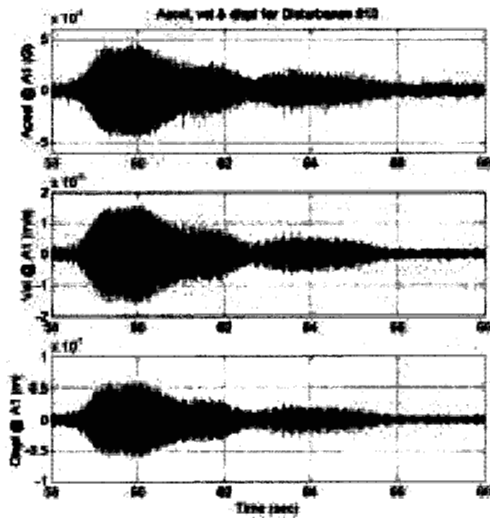


FIG. 9: Acceleration, velocity & displacement for narrowband Disturbance #13 (boom accelerometer A1).

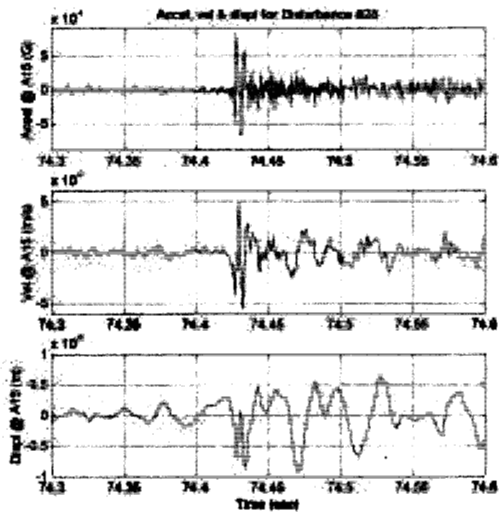


FIG. 10: Acceleration, velocity & displacement for impulsive event at the onset of Disturbance #20 (SPAS accelerometer A15).

Figure 8 shows time traces for an impulsive disturbance felt most significantly on SPAS-mounted channel A15. These time traces were less corrupted by low-frequency electronic noise, so a high-pass filter with corner frequency at 0.5 Hz was used in the integration process. In the Event Catalog document<sup>13</sup>, this broadband disturbance (labeled Disturbance #12) was suspected to have

had its source on the Astro-SPAS, or at the spacecraft/boom interface. This disturbance source localization was made based on the relative amplitudes of the measurements and the relative starting times of the event on different channels. The  $700 \mu\text{g}$  acceleration jump seen on this channel integrates to velocity and displacement peaks of roughly  $40 \mu\text{m/s}$  and  $3 \mu\text{m}$ , respectively. Impulsive disturbances of this magnitude are of particular concern for an instrument with stringent positional stability requirements, such as SIM.

Acceleration, velocity and displacement time histories of a 43 Hz narrowband disturbance labeled as Disturbance #13 in the Event Catalog<sup>13</sup> are plotted in Figure 9. This event introduces a peak displacement greater than 50 nm, at boom tip accelerometer A1, the worst-case boom sensor location. The RMS acceleration, velocity and displacement computed over the duration of this disturbance are  $157 \mu\text{g}$ ,  $5.5 \mu\text{m/s}$  and 21 nm, respectively. This response likely corresponds to excitation of a coupled SPAS/boom mode. The FE model predicts a mode in which boom torsion is coupled with boom bending and A/S motion around 41.2 Hz (see Table 1). The source of this disturbance has not yet been identified.

The integration and filtering process was also applied to the impulsive event which appears to lead into Disturbance #20, the increase in background noise level attributed to a time-varying frequency content band (this appears as a "persistent crackling" starting at 74 sec in the time histories of Figure 6). The resulting time histories for SPAS-mounted accelerometer A15 are plotted in Figure 10. Peak values of  $800 \mu\text{g}$ ,  $5 \mu\text{m/s}$  and 7 nm are seen, in the acceleration, velocity and displacement traces, respectively. It should be noted that the nature of the source for Disturbance #20 (electronic vs. structural) is still in question, however.

Time traces from a representative impulsive disturbance suspected to have had its source at a boom mechanism are shown in Figure 11. Response to this Disturbance #28 is only clearly seen in the acceleration time history, reaching a peak of roughly  $400 \mu\text{g}$ . The velocity and displacement traces are dominated by lower-frequency content.

Toward the end of the quiescent period, one set of thrusters was deliberately fired, in order to characterize the response of the system. Acceleration, velocity and displacement time histories for one thruster burst (as measured on the IPEX boom at A13) are plotted in Figure 12. Peak accelerations of 1.2 mg are achieved; integration and filtering of the signal yields peak velocities

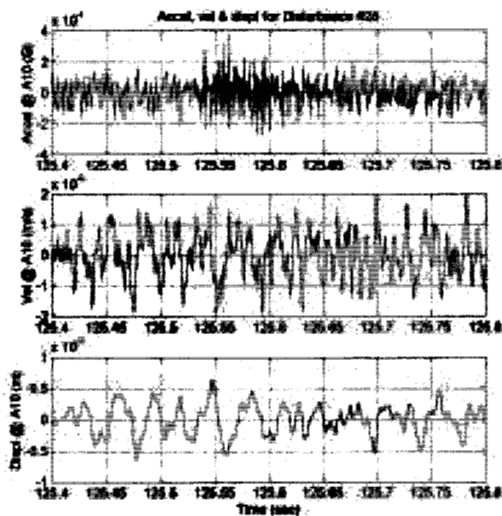


FIG. 11: Acceleration, velocity & displacement for impulsive Disturbance #28, with assumed boom source (boom accelerometer A10).

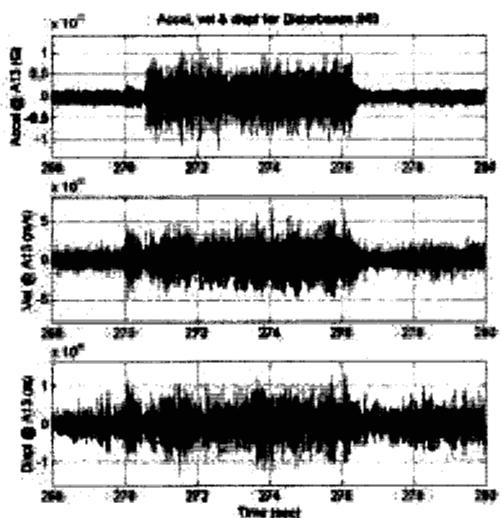


FIG. 12: Acceleration, velocity & displacement for thruster Disturbance #43 (boom accelerometer A13).

and displacements of  $6.5 \mu\text{m/s}$  and  $12 \text{ nm}$ , respectively. Taking the RMS of each trace over the duration of the thruster burst yields  $300 \mu\text{g}$  RMS acceleration,  $1.7 \mu\text{m/s}$  RMS velocity, and  $4 \text{ nm}$  RMS displacement. Finally, it should be noted that the thruster pulses from the 5-minute quiescent period were not representative of the worst-case thruster disturbances experienced on-orbit.

One of the subsequent 5-minute data segments (addressed in Section 4.2) reflects peak thruster response accelerations on the order of  $7.5 \mu\text{g}$ ,  $20 \mu\text{m/s}$  of peak velocity and  $50 \text{ nm}$  of peak displacement.

## 4.2 Experiments Following the Quiescent Period

At the end of the quiescent period experiment, the gyros were turned back on so the A/S could regain its attitude control. The quiescent period data was downloaded to the tape recorder, and the subsequent experiment was started roughly 10 minutes later. The A/S and the boom were still in full sun illumination, and no thermal transitions occurred during the next 2 recording periods. The segment immediately following the quiescent period was supposed to be fully dedicated to various thruster pulsing sequences for disturbance propagation and boom response analysis. However, because of an unexpected anomaly in the telecommunication system, no commands could be sent up to the A/S after the first thruster pulse sequence. Consequently, the remaining 4.5 minutes of the experiment became in essence another quiescent listening period with the gyros functioning in the background (a.k.a., "quiescent gyro experiment"). This glitch allowed the quiescent period analysis to be extended beyond the originally planned experiment. Fortunately, telecommunications were quickly recovered, and the thruster pulsing sequence was performed in the following experiment sequence (a.k.a. "thruster pulsing experiment"). Segments of these two experiments are presented herein for comparison to the quiescent period results.

Figure 13 illustrates a typical time history and spectrogram from an accelerometer on the boom (A1 at the tip of the boom, in the lateral z-direction) during the quiescent gyro experiment. A thruster pulsing sequence is seen between 21 sec and 27 sec, producing a broadband response on the boom. The gyros produce disturbances at  $505 \text{ Hz}$  and  $800 \text{ Hz}$ , which are aliased down to  $495 \text{ Hz}$  and  $200 \text{ Hz}$ , seen in the spectrogram as straight, steady lines. A consistent ringing at  $30 \text{ Hz}$  is present in the data, presumably associated with the boom's torsional mode. This persistent ringing was also present throughout the quiescent period. Another predominant disturbance is the periodic pulse occurring at approximately 14.4-second intervals, presumably from the tape recorders. These disturbances cause boom response around  $70 \text{ Hz}$ ,  $90 \text{ Hz}$ ,  $170 \text{ Hz}$ , and  $190 \text{ Hz}$ . It is also interesting to note that other intermittent microdynamic impulses still occur, but these are less frequent in time than during the quiescent period. In particular, an event at around 153

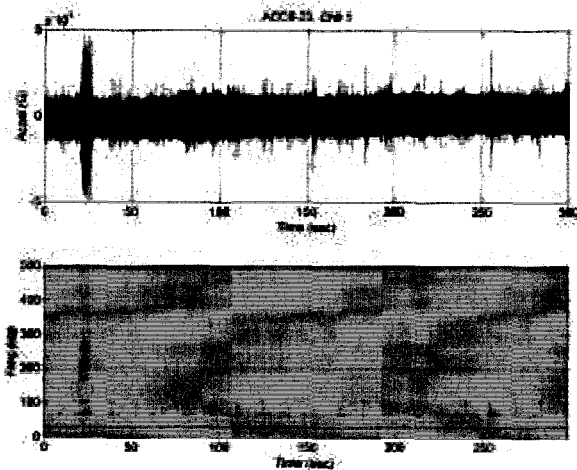


FIG. 13: Typical time history and spectrogram from the quiescent gyro period (boom accelerometer A1).

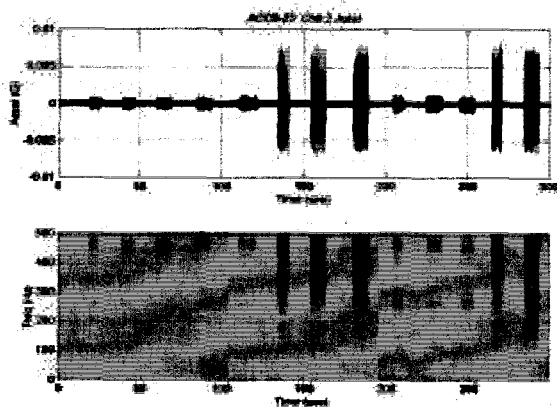


FIG. 14: Typical time history and spectrogram from the dedicated thruster pulsing experiment (boom accelerometer A2, in the axial direction at the tip of the boom).

sec is comparable to the quiescent period Disturbance #13, with a predominant response frequency around 42 Hz. Other significant creaks are seen at 175 sec and 255 sec.

The broadband [0-500Hz] RMS response to the thruster pulsing sequence in the quiescent gyro period is largest (approximately 285  $\mu\text{g}$ ) at accelerometer A13, located near the base of the boom in the transverse Z-direction. The broadband RMS of the boom response from the gyro disturbances alone is about 50 $\mu\text{g}$  to 80 $\mu\text{g}$  in the lateral directions and 120 $\mu\text{g}$  in the axial direction. The lat-

eral response is only slightly higher than the RMS response without the gyros, as recorded during the first portion of the quiescent period experiment. The RMS gyro response at accelerometer A16 (located near a gyro assembly) is roughly 300  $\mu\text{g}$ .

Another significant feature is the disappearance of the "persistent crackling" noise which predominated the end portion of the quiescent period data (Disturbance #20 in the Event Catalog<sup>13</sup>). This crackling was characterized in the spectrograms as a time-varying frequency strip with regularly occurring jumps, and it was even recorded in the disconnected channel 20. None of the data recorded during the quiescent gyro segment identified this type of disturbance.

A typical plot of the boom response during the thruster pulsing experiment is presented in Figure 14. There are two redundant sets of cold-gas thrusters on-board the A/S to provide rotational attitude control. Each set contains six 100-mN (0.0225-lb) thrusters. The thrusters are located at the keel and at each end of the top pallet. The intent of this experiment was to pulse different sets of thrusters in different directions at different duty cycles to correlate a deterministic forcing function input to the boom's dynamic response. The amplitude of the thrust cannot be varied, and is always set at 100 mN.

The amplitude and frequency content of boom response varies with the characteristics of the pulsing function, as would be expected. The boom is most sensitive to thrusters pulsing in the z-direction with maximum response amplitudes in the tens of millig's peak-to-peak. Furthermore, a 40 Hz transient is observed just after 100 sec, similar to Disturbance #13 from the quiescent period.

## 5 CONCLUSIONS

Analysis of the quiescent period, the quiescent gyro period and the thruster pulsing sequences has yielded numerous interesting findings. In this section, these findings are summarized.

A catalog of the various disturbances seen during the quiescent period has been compiled<sup>13</sup>, which reveals a wide variety in the types of events recorded. These events include steady-state disturbances, transient disturbances, and disturbances with time-varying frequency content. The microdynamic events occur most frequently right after the night-to-day transition. Later in the time history, less microdynamic activity is observed.

The occurrence of impulsive microdynamic-level disturbances has been demonstrated on-orbit. The analysis to date suggests that some of these events were thermally-induced structural disturbances. IPEX-2 represents the first known, deliberate attempt to characterize such disturbances on-orbit, though on-orbit operational data from the Hubble Space Telescope has shown evidence of impulsive thermally-induced structural phenomena<sup>8</sup>, and a demonstration of thermal creak observed in a ground laboratory environment has been previously documented<sup>6</sup>.

A preliminary localization of the source of the impulsive events was attempted, based on apparent delays in the time of occurrence of the events at different sensor locations across the structure. Some of the events seem to have originated on the Astro-SPAS or at the SPAS/boom interface, and others seem to have originated on the IPEX boom.

A quantitative characterization of the identified disturbances was performed:

- The quiescent period thruster pulses induce RMS response on the boom of 300  $\mu\text{g}$  in acceleration, 2  $\mu\text{m/s}$  in velocity and 5 nm in displacement. The worst-case firing direction in the thruster pulsing sequence following the quiescent period resulted in RMS response amplitudes on the order of 1.5 mg, 5  $\mu\text{m/s}$  and 15 nm.
  - During the quiescent gyro experiment, the response to the gyros was felt at 200 Hz and 495 Hz (aliased down from 800 Hz and 505 Hz, respectively). The broadband RMS of the boom response to the gyros is about 50  $\mu\text{g}$  to 80  $\mu\text{g}$  in the lateral directions, and 120  $\mu\text{g}$  in the axial direction.
  - One type of impulsive disturbance, associated with the flight data recorder, was found to occur every 14.4 seconds. The response to these disturbances was felt most significantly on the boom accelerometers, reaching peak acceleration, velocity and displacement levels of 300  $\mu\text{g}$ , 5  $\mu\text{m/s}$  and 15 nm, respectively.
  - Narrowband 43 Hz disturbances were seen in the data, building up and decaying over a period of 5 seconds or so. Such events occurred twice in the quiescent period experiment, and at least once in both the quiescent gyro experiment and the thruster pulsing experiment. Peak amplitudes of over 400  $\mu\text{g}$ , 15  $\mu\text{m/s}$  and 50 nm were seen in response to these narrowband disturbances.
- Finally, numerous broadband, impulsive events were identified as possible thermal creaks. The response levels seen for these disturbances vary widely, but in general, peak accelerations in the range from 300  $\mu\text{g}$  to 700  $\mu\text{g}$  were recorded. Peak integrated velocities were generally on the order of 5  $\mu\text{m/s}$ , and the peak integrated displacements were generally less than 50 nm. These integrated velocities and displacements were often dominated by low-frequency noise, but at least one event (suspected to have had its source on the A/S or at the SPAS/boom interface) introduced peak velocities and displacements on the order of 40  $\mu\text{m/s}$  and 3 microns, respectively.

The existence of such impulsive microdynamic phenomena suggests that precision optical spacecraft requirements expressed in terms of RMS quantities may be inadequate. Short transient disturbances, which are insignificant in a time-averaged, RMS sense, may nonetheless be unacceptable if they cause a telescope's optics to lose their metrology lock, for example. Requirements expressed in terms of peak perturbation levels and rates should be considered.

## **6 ACKNOWLEDGEMENTS**

This work was performed at the Jet Propulsion Laboratory, California Institute of Technology, under contract with the National Aeronautics and Space Administration. Michel Ingham would like to acknowledge the support and guidance of Prof. David Miller at the MIT Space Systems Laboratory.

## **REFERENCES**

- <sup>1</sup> Levine, M.B., "The Interferometry Program Flight Experiments: IPEX I & II", Proc. SPIE Astronomical Telescopes and Instrumentation Conference, Kona, HI, March 1998, Paper 3350-14.
- <sup>2</sup> Levine, M.B., "Microdynamic Behavior of a Joint Dominated Structure On-orbit", 40th SDM Conference, St. Louis, MO, April 12-15, 1999, AIAA paper #99-1267.
- <sup>3</sup> Hinkle, J.D. and Peterson, L.D., "An Experimental Investigation of Roughness-Induced Microslip in Metallic Interfaces", 40th SDM Conference, St. Louis, MO, April 12-15, 1999, AIAA paper #99-1382.
- <sup>4</sup> Hachkowski, M.R., Peterson, L.D. and Lake, M.S., "Analytical Model of Nonlinear Hysteresis Mechanisms

in a Rolling Element Joint", 40th SDM Conference, St. Louis, MO, April 12-15, 1999, AIAA paper #99-1268.

<sup>5</sup> Hardaway, L.M.R. and Peterson, L.D., "Microdynamics of a Precision Deployable Optical Truss", Proceedings of the SPIE Annual Meeting, Denver, Colorado, July 1999, SPIE paper #3785-01.

<sup>6</sup> Ingham, M., Kim, Y., Crawley, E., McManus, H., and Miller, D., "Experimental Characterization of Thermal Creak Response of Deployable Space Structures", 40th SDM Conference, St. Louis, MO, April 12-15, 1999, AIAA paper #99-1269.

<sup>7</sup> Kim, Y.A., McManus, H.L., and Miller D.W., "Thermal Creak Induced Dynamics of Space Structures", Ph.D. Thesis, Dept. of Aeronautics and Astronautics, MIT, Cambridge, MA, February 1999, SERC Report #14-98.

<sup>8</sup> Blair, M., and Sills, J., "Hubble Space Telescope On-Orbit System Identification", Proc. 12th International Modal Analysis Conference, Honolulu, HA, February 1994, pp. 663-669.

<sup>9</sup> Hinkle, J.D., Warren, P.A., and Peterson, L.D., "Design and Testing of an Optical Precision Deployment Latch", 40th SDM Conference, St. Louis, Missouri, April 12-15, 1999, AIAA paper #99-1270.

<sup>10</sup> Lake, M.S., Fung, J., Gloss, and K., Liechty, D.S., "Experimental characterization of hysteresis in a revolute joint for precision deployable structures", 38th SDM Conference, April 7-10, 1997, AIAA paper #97-1379.

<sup>11</sup> Ingham, M., and Levine, M., IPEX-2 Flight Configuration Modeling Task Report, Jet Propulsion Laboratory Document JPL D-16986, March 16, 1999.

<sup>12</sup> Peng, C.-Y., Levine-West, M., and Tsuha, W., Interferometry Program Experiment IPEX-II Pre-flight Ground Modal Test and Model Correlation Report, Jet Propulsion Laboratory Document JPL D-14809, September 19, 1997.

<sup>13</sup> Ingham, M., and Levine, M., IPEX-2 Quiescent Period On-Orbit Event Catalog, Jet Propulsion Laboratory Document JPL D-17821, May 15, 1999.

<sup>14</sup> Ingham, M., and Levine, M., IPEX-2 Flight Data Analysis: Quiescent Period Report, Jet Propulsion Laboratory Document JPL D-17912, June 30, 1999.